Karnataka University Journal of Science 54(3), (2023), 11–18

Karnataka University Journal of Science

ISSN: 0075-5168

Research Article

# Bioadsorption of Oxyanions of Chromium using Bionanomaterial: Thermodynamics and Kinetic Studies

**G Jaishree[1], G Divya[1], T Siva Rao[1,*], M L Prasanna Chippada[1]**

[1] *Department of Chemistry, Andhra Unversity, Vishakapatnam, 530003, India*

ARTICLE INFO

*Article history:*
Received 29.10.2022
Accepted 07.07.2023
Published 01.11.2023

* *Corresponding author.*
T Siva Rao
sivaraoau@gmail.com

https://doi.org/10.61649/kujos/v54i3.jaishree

ABSTRACT

This study focused on fabricating an activated bionanomaterial derived from *Calotropis procera* stem through ball milling. The resulting bionanomaterial was characterized using FTIR, SEM, and BET surface area analysis. Notably, BET analysis revealed a significant increase in surface area (578 m2/g). SEM images exhibited an uneven surface with larger holes and cave-like openings. FTIR analysis indicated the presence of -OH groups on the bionanomaterial's surface. The activated bionanomaterial was then utilized for Cr(VI) adsorption experiments, and optimal adsorption parameters were determined as pH 2, contact time of 180 minutes, adsorbent dosage of 3 g, initial Cr(VI) concentration of 40 ppm, and temperature of 60°C. Thermodynamic analysis demonstrated positive ΔH and negative ΔG values, suggesting an endothermic and spontaneous adsorption process. The adsorption kinetics followed a first-order reaction, and the experimental data aligned well with the Langmuir adsorption isotherm.

**Keywords:** Activated Carbon; Bioadsorption; Ball milling; Adsorption isotherms; Thermodynamics; Kinetic studies of adsorption

## 1 INTRODUCTION

Rapid urbanization and industralisation posed a threat to ecosystem by release of heavy toxic metals such as arsenic , chromium, cadmium, lead and mercury into the waste water streams [1]. Chromium exists in polyvalent states among which $Cr^{6+}$ and $Cr^{3+}$ are stable form [2]. $Cr3^{+}$ present as an essential metal ion in humans where as $Cr^{6+}$($CrO_4^{2-}$) and dichromate ($Cr_2O_7^{2-}$), highly toxic at all concentrations due its strong oxidizing properties showing detrimental effects by oxidizing the DNA, Proteins and certain other biomolecules [3]. High chromium exposure causes cancer of the digestive tract and lungs [4]. Waste water receives hexavalent chromium contaminations from industrial discharges of electroplating, mining, fertilizer, cement, photography industries, dyeing, and leather tanning [5]. Maximum permitted limit of total chromium as recommended by WHO in drinking water is 50 $\mu$g/L [6]. There are many advance procedures adopted for treatment of them in waste water such as ion exchange, chemical precipitation, electrocoagulation, electrochemical method, biological treatment, physical filtration process using nanofiltration, microfiltration and adsorption [7]. Among these Adsorption is found to be efficient even at low Chromium concentration, due to its some of the adventitious properties [8]. Activated carbon (AC) is renowned for its effective adsorption derived from its high surface area and microporous characteristics [9]. Inspite of these merits there are some economical and technical challenges associated with them which includes high operational costs, high temperature requirements and constraints in terms of selectivity [10]. Fabrication of AC's under laboratory feasible conditions is a summon to researchers now a days. In this context, researchers have developed substitutes evolved from agricultural wastes such as bamboo, sugarcane bagasse, nut shells, cotton stalks, pine cones, walnut shells, peanut shells, and tobacco residue but owing to the high temperature required for conversion resulting in high ash content [11, 12]. The activated carbon derived from plant part such as stem, leave, bark, root, flower, fruit peel, has an added advantage over agricultural waste derived AC's as they are mainly composed of cellulose [13], hemicelluloses, lipids, lignin [14], sugar, water, hydrocarbon, starch, protein, and

many functional groups with low temperature requirement.

This study aims for the synthesis of Bionanomaterial derived from *Calotropis procera* stem and evaluation of its adsorption efficiency for removal of Cr(VI), the suitability of experimental data were studied using best fit adsorption isotherm models.

## 2 EXPERIMENTAL

### *2.1 Biomaterials, Chemicals and Solution preparation*

*Calotropis procera* stem obtained locally was taken as a precursor for preparation of activated carbon. Freshly prepared HCl and NaOH were taken to adjust the pH during adsorption studies. Stock (1000 ppm) solution of $K_2CrO_4$in deionised water, were taken as a source precursors for Cr(VI) in slight acidic conditions. Metal ion concentration was varied in the range from (5ppm-100ppm) obtained by dilution of stock solutions which were further used for batch adsorption studies.

### *2.2 Instrumental techniques employed for Ballmilling and characterisational analysis*

Ballmilling is a green mechanochemical approach, generally employed in low temperature alloy processing. Here in we have utilized this technique for the scissoring of as obtained activated carbon which is a prime requisite for efficient adsorption of toxic metals owing to increase in surface area. High Energy Ball mill (EMAX, Retsch, INDIA) was used for ballmilling the biomaterial to nanosize, Orbital Shaker (EIS 35S LABZEE BIOTECH, INDIA)was used for shaking in adsorption of metal ion.FTIR spectra of the sample were recorded in the frequency range 4000-400 cm1 for detection of functional groups introduced during the process using The JASCO 4100 FTIR spectrometer (Jasco International, Tokyo, Japan) in transmission mode using the KBr pellet method was used to analyze the bionanomaterial. The morphology of the material was investigated using a ZEISS SIGMA FE-SEM scanning electron microscope equipped with an EDX spectrophotometer. The Brunauer-Emmett-Teller (BET) method was employed with a Quanta chrome Nova 2200 E System surface area analyzer to calculate the pore volume, size, and surface area using N2 adsorption-desorption isotherm at 77.3 K.Varian SpectrAA 800 Atomic Absorption Spectrometer with Zeeman background correction and a GTA 100 graphite furnace. A chromium hollow cathode lamp (Varian) was utilized for adsorption tests to determine the concentration of Cr(VI).

#### *2.2.1. Conversion of Biomass into Activated Carbon*

The fresh *Calotropis procera* stem was collected from the local shrub available in campus premises of Andhra University, Vishakapatnam, India. The stem was made into small pieces and then rinsed with deionised water to remove dirt or other particulate matter if any, shade dried the pieces for 2-3 days, then finely grounded the pieces. The as obtained grounded biomass was taken in crucible and carbonised in muffle furnace at $190^0$C for 24 hrs was then stored in air tight container kept in desiccator to avoid absorption of moisture.

In order to achieve the best adsorption performance and high surface area. The as obtained carbonized nanomaterial was further scissored using High Energy Ball milling. Further the carbonized bionanomaterial was subjected to proximate and structural analysis using ISI standard procedure [3rd Revision,2004] and best parameter value obtained owing to low ash content , high ion exchange capacity, low apparent density and high total carbon content desirable for high grade activated carbon as observed in Table 1. It can be estimated from the phenol value(95.00 mg/g) and methylene blue value(29.0 mg/g), the sufficient adsorption capacity of bionanomaterial towards positive metal ions.

**Table 1:** Proximate chemical and textural analysis of bionanomaterial

| Parameter Analysed | Value of each parameter |
|---|---|
| Moisture content (%) | 7.60 |
| Matter soluble in acid (%) | 0.15 |
| Total carbon (%) | 72.4 |
| Ash content (%) | 25.64 |
| Matter soluble in water (%) | 0.20 |
| Ion exchange capacity(meqts/ gm) | 1.18 |
| Iron (%) | 0.063 |
| Surface area (sec.) ($m^2$/gm) | 578 |
| Phenol number (mg/g) | 95.00 |

Adsorption experiments were carried out by the adding desired concentrations of metal ion solutions and adsorbent dose in 150mL conical flasks maintained at a particular optimized pH and were agitated using EIS 35S Orbital shaker with a rotating speed of 350 rpm till equilibrium is achieved for 3hrs and then the aliquots were collected at different time intervals and analysed for change in concentration of metal ion with time using AAS. The formula can be employed to calculate the percentage removal of metal ions.

$$\% \text{ Adsorption } = \frac{C_i - C_f}{C_i} \times 100 \quad (1)$$

where Ci -initial concentration and Cf - final concentration of the metal ion.

Different parameters have been studied and optimised to obtain the best adsorbent dosage concentration, pH, metal ion concentration , temperature and contact time by continuously varying one parameter keeping other parameters constant.

## 3 RESULTS AND DISCUSSION

### *3.1 Characterizational analysis of Bionanomaterial*

#### *3.1.1. FTIR Analysis*

Figure 1 depicts the FTIR spectra of Bionanomaterial.The peak values at different band positions corresponds to the

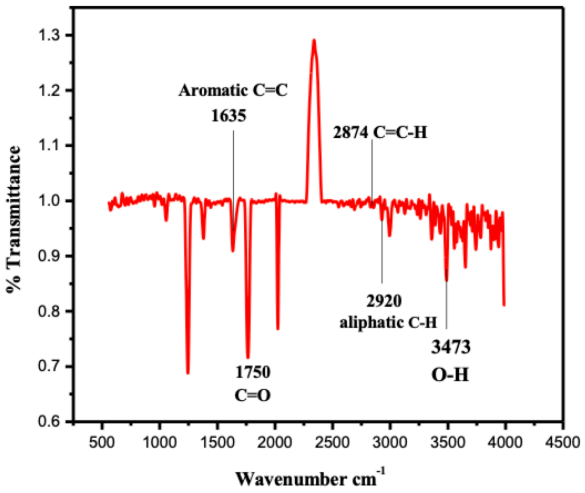


**Figure 1:** FTIR analysis of Bionanomaterial

different functional groups which accounts for the structural and chemical characteristics. The intense peak observed at 3473 $cm^{-1}$ attributes to the surface hydroxyl group of carboxylic, alcohol or $H_2O$ adsorbed on the surface [15], the band at 2920 $cm^{-1}$ [16] and 2874 $cm^{-1}$ [17] corresponds to the methyl and methylene C-H bonds, respectively.The additional peak at 1635 $cm^{-1}$derived from the aromatic C=C group proves the presence of aromatic rings in the as obtained bionanomaterial [18].The corresponding stretching frequencies of functional groups contributes to facilitated adsorption of Cr(VI) on bionanomaterial.

### *3.1.2. BET Surface area analysis*

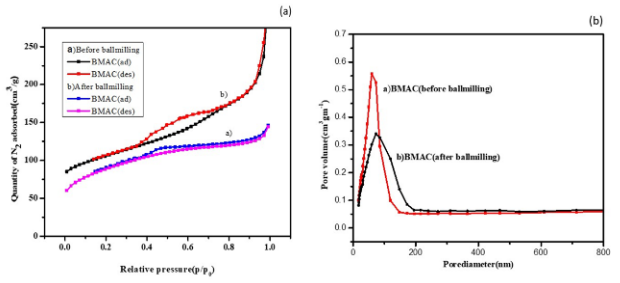


**Figure 2:** a) $N_2$ adsorption–desorption isotherms and b) BJH pore size distribution curve, of Bionanomaterial.

The $N_2$ Adsorption Desorption Isotherms and BJH pore size distribution curve of Bionanomaterial,indicating $H_2$ hysterisis loop with type IV isotherm characteristic of the ordered macroporous structure (Figure 2 a & b). Before ballmilling the BET surface area was found to 302 $m^2/g$ with pore volume 0.256 $cm^3/g$ and pore size 4.8nm which after ballmilling BET surface area 578 $m^2/g$ pore volume 0.342 $cm^3/g$ and pore size 62.40 nm found to increase confirmed the scissoring of bionanomaterial using Ballmill.

### *3.1.3. SEM EDX analysis*

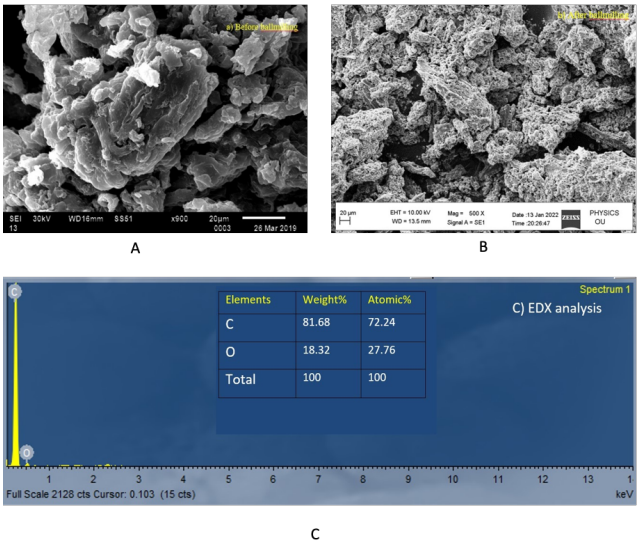


**Figure 3:** SEM images of Bionanomaterial a) before ballmilling b)after ballmilling at same resolutionand c) EDX analysis

The shape and surface morphology of bionanomaterials before and after Ballmilling were compared and are shown in (Figure 3 a & b). It vividly demonstrates the irregular surface, larger holes, and cave-like apertures on the surface. This reflects the more pronounced porosity character of the bionanomaterial after ballmilling, which results in better adsorption. This type of structure is obvious due to the presence of functional groups that allow metal ions to be trapped. The elemental analysis (Fig. 3c) confirms the existence of Carbon and Oxygen.

## *3.2 **Best optimized parameter for adsorption of Cr(VI) on Bionanomaterial***

### *3.2.1. Effect of solution pH*

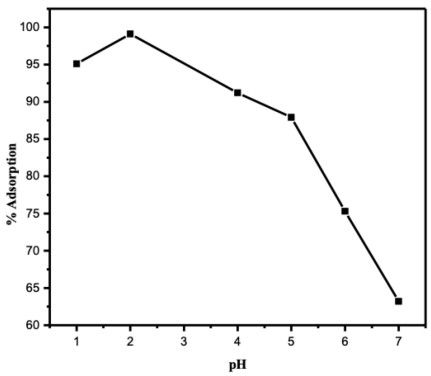


**Figure 4:** Effect of pH for Cr(VI) adsorption (adsorbent dosage 3.0 gm, duration 180 min)

The solution pH highly influence the adsorption property owing to the existence of dominant species at particular pH. At acidic pH the predominant species is hydrogen chromate ($HCrO_4^-$)and high $H^+$ concentration masking the negatively charged surface hydroxyl group and neutralizes it which inturn facilitates the diffusion of ($HCrO_4^-$) on bionanomaterial [19]. Hence, It can be inferred from the (Fig. 4), that the maximum adsorption (99%)was achieved at pH 2 beyond which(>2) there is decrement in the $H^+$ ion concentration and an electrostatic repulsion exist between the negatively charged chromate and $-OH^-$ groups [20]. At pH 1,availability of excess protons promote the reduction of Cr(VI) to Cr(III), which led to competition between H+ and Cr(III) for surface charged groups [21]. Hence, adsorption seemed less at pH 1 as compared to pH2. Thus pH 2 was optimized for further parameter studies.

### 3.2.2. *Influence of Contact Time and Catalyst dosage*

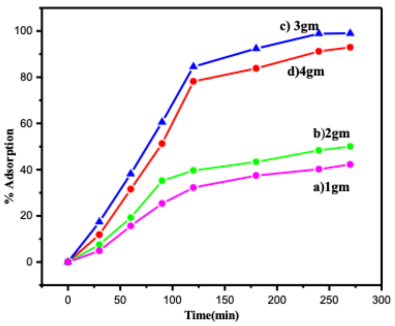


**Figure 5:** Effect of contact time on % adsorption of metal ion (40ppm HgII)

The influence of contact time and catalyst dosage on adsorption of Bionanomaterial was studied in the range from 0 to 300 min. The experiments were carried out using 40ppm Cr(VI) ion concentration with carbon dosage varying from 1-5 gms with agitation speed 250 rpm maintained at pH2 at room temperature. The results revealed the rapid increase in % adsorption for all the catalyst dosage then diminished gradually to attain equilibrium with in 180 min which is presented in Fig. 5. This may be resulted from the fact that there is direct relationship between the metal ion concentration and time, lower the concentration lesser the time needed to attain equilibrium. Comparatively Among all the catalyst dosage 3gm shown to have high adsorption efficiency this is may be due to electrostatic repulsion exist between $Cr_2O_7^{2-}$ and surface charged groups of bionanomaterial. However as time proceeds the stabilization of adsorption due to saturation of active sites takes place. Taking into consideration the above facts the contact time was optimized at 180min and catalyst dosage 3gm for subsequent parameters study.

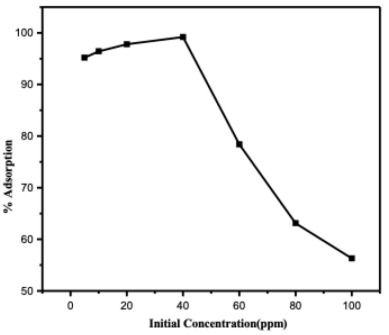


**Figure 6:** Effect of initial concentration of Cr(VI) (Adsorbent dosage 3.0gm, contact time 180 min and pH 2)

### 3.2.3. *Influence of initial metal ion concentration*

Figure 6 shows the interdependency of Adsorption (%) with initial concentration of Cr(VI) ion. The initial metal ion concentration was increased in the range from 5ppm to 100ppm optimising other parameter such as contact time(180 min), adsorbent dose 3.0gm,solution pH maintained at 2. The adsorption seemed to be increased from 5 to 40ppm beyond which it decreased. At low metal ion concentration the availability of adsorptive site is more but as concentration of metal ion increases the charge saturation attains at 40ppm beyond which due to non-availability of effective reactive space the adsorption decreases.

### 3.2.4. *Influence of temperature for Cr(VI adsorption)*

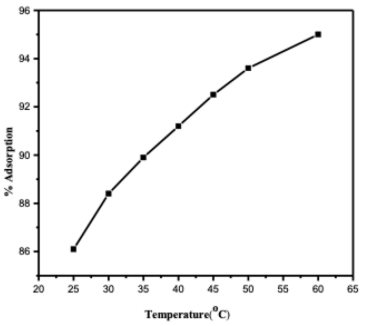


**Figure 7:** Effect of temperature on adsorption (adsorbent dosage 3.0 gm, duration 180 min, pH 2)

Influence of temperature on adsorption was studied ranging from 20-60$^0$C with increment of 5$^0$ C and results were depicted in Fig.7,which referred that there is a direct relationship exists between the adsorption efficiency and temperature which can be attributed from the fact that due to increased mobility and solubility the extent of adsorption increases [22]. Moreover, the broaden and deepen pore size and structure facilitate the adsorption through a phenomenon known as activated diffusion [23].

The promoted diffusion of metal ion evident for the endothermic nature of reaction.

Hence at 180 min, Adsorbent dose 3gm, Cr(VI) ion concentration 40 ppm, solution pH 2 maintained at temperature $60^0$C. The rate of adsorption of Cr(VI) ion was found to be 99%.

Study of thermodynamic parameters.

The values H and S were calculated using the following formula

$$\ln K_d = \frac{\Delta S}{R} - \frac{\Delta H}{RT} \tag{2}$$

Where: S = entropy change for the procedure

H = change in enthalpy of the process.

R = gas constant

Using the equation (3), the distribution coefficient (Kd) on the surface of activated charcoal was calculated.

$$K_d = \frac{C_i - C_e}{C_e} \times \frac{V}{m} \left(mLg^{-1}\right) \tag{3}$$

The variations in free energy (G) for the specific adsorption were also calculated using the following equation (4),

$$\Delta G = -RT \ln K_d$$

**Table 2:** Adsorption studies of Cr(vi) ion (T as function)

| T (K) | 1/T ($K^-x10^{-3}$) | $K_d$ ($mLg^{-1}$) | Ln$K_d$ | ΔG ($kJmol^{-1}$) |
|---|---|---|---|---|
| 295 | 3.38 | 41.29 | 3.72 | -29.58 |
| 305 | 3.27 | 50.79 | 3.92 | -30.58 |
| 310 | 3.22 | 59.33 | 4.08 | -31.08 |
| 315 | 3.17 | 69.09 | 4.23 | -31.58 |
| 320 | 3.1 | 82.20 | 4.41 | -32.08 |
| 325 | 3.07 | 97.50 | 4.57 | -32.59 |
| 330 | 2.9 | 126.6 | 4.84 | -33.09 |

The thermodynamic quantities H, S, and G of Cr(VI) ion adsorption on activated carbon were determined from the Kd values using the aforementioned equations. The slope and intercept of the linear variations of ln Kd with the reciprocal of temperature (Fig. 8) were used to calculate H and S, which were 20.56 and 100.34 kJ mol-1, respectively. The rise in adsorbate diffusion between the external boundary layer and internal pores of the adsorbents implies that the process is endothermic [24].The computed values of the free energy of specific adsorption, delta G, at various temperatures are shown in Table 4. The adsorption process is more spontaneous when delta G is negative.

### *3.3 Best Adsorption isotherm fit model studies*

#### *3.3.1. Langmuir Adsorption isotherm*

It describe a monolayer adsorption of adsorbate onto a homogeneous adsorbing surface characterized by uniform binding sites . It further postulates the absence of interaction between the adsorbed molecules while undergoing adsorption process. The Langmuir isotherm is expressed in Eq. (5)

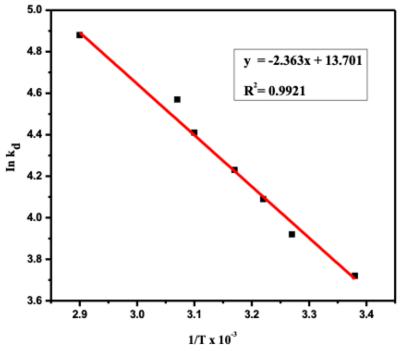


**Figure 8:** Plot of Ink$_d$ Vs 1/T the slope and intercept gives delta H and delta S respectively

$$q = \frac{q_{\max} b C_{\max}}{C_{eq} C_{\max}} \tag{5}$$

Where,

$q_{max}$ = maximum monolayer coverage capacity (mg/g)

q = the amount of metal adsorbed per gram of the adsorbent at equilibrium (mg/g).

b= Langmuir isotherm constant (L/mg).

$C_{eq}$ = the equilibrium concentration of adsorbate ($mg/L^{-1}$)

The linear form of Langmuir equation derived from (5) and is given in (6)

$$1/q = \frac{1}{q_{\max}} + \frac{1}{(C_{eq} q_{\max} b)} \tag{6}$$

The values of q and b were computed from the slope and intercept of the Langmuir plot of $1/C_e$ versus $1/q_e$ (Fig.9)and The experimental data fits the isotherm adequately and the parameters have been tabulated in Table 3.

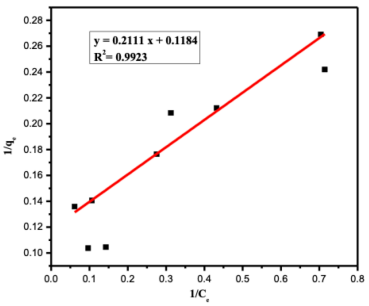


**Figure 9:** Langmuir adsorption isotherm plot for the adsorption of Cr (VI) on bionanomaterial

### *3.3.2. Freundich Adsorption Isotherm*

The Freundlich isotherm can be derived from the Langmuir isotherm by presuming that the adsorbent contains sites with varying affinities for different adsorbates. This model is particularly well suited to explaining multilayer adsorption on a heterogeneous surface with a non-uniform distribution of adsorption heat and affinities.

The Freundlich equation, which represents this relationship, is as follows:

qe = KC1/n

In this equation, 'K' indicates the adsorbent's capacity (mass of adsorbate /the mass of adsorbent) and 'n' is a measure of how the affinity for the adsorbate changes with adsorption density. It is vital to remember that when n > 1, affinities tend to decrease as adsorption density increases. Using the linearized form, it is possible to calculate the coefficient of K and n.

$$\log qe = \log K + 1/n \log Ce \quad (8)$$

Figure 10 shows the calculated and plotted values for these parameters. From the Figure, it can be concluded that $R^2$ = 0.8348.

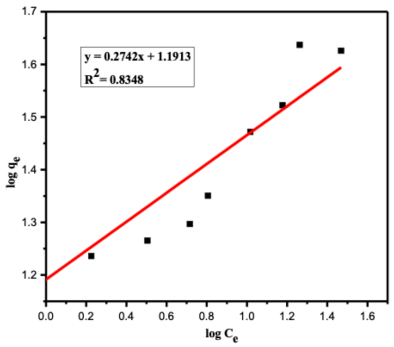


**Figure 10:** Freundich adsorption isotherm plot for the adsorption of Cr (VI) on bionanomaterial

### *3.3.3. Section Headings*

There is a factor in the Temkin isotherm that explicitly accounts for adsorbent–adsorbate interactions. It further suggests that, due to interaction, the heat of adsorption of all molecules in the layer would decrease linearly if the exceedingly low and high concentration values were disregarded. The expression for the tempkin isotherm can be written as

$$q_e = B \ln (AC_e) \quad (9)$$

where B = RT/b, b is tempkin constant and A is equilibrium binding constant.

The linear form of Tempkin equation can be expressed as

$$q_e = B \operatorname{Ln} A + B \operatorname{Ln} CC_e \quad (10)$$

A plot of $q_e$ against $\ln C_e$(Fig.11) gives the value of A and B. All the tempkin parameters are tabulated in Table 3.

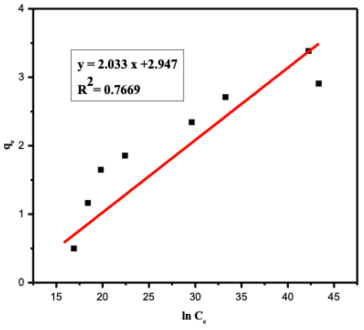


**Figure 11:** Tempkin adsorption isotherm plot for the adsorption of Cr (VI) on bionanomaterial

**Table 3:** Langmuir, Freundlich and Tempkin parameter values

| Isotherm | Parameters | Value |
|---|---|---|
| Langmuir | $q_{max}$(mg/g) | 3.20 |
| | b(L/mg) | 0.126 |
| | $R^2$ | 0.992 |
| Freundlich | 1/n | 0.378 |
| | K(mg/g) | 3.297 |
| | $R^2$ | 0.834 |
| Tempkin | A(L/g) | 5.20 |
| | B(J/mol) | 2.124 |
| | $R^2$ | 0.767 |

### *3.4 Calculation of the order of the Adsorption reaction*

The rate constant (k) for the adsorption of Cr (VI) ions onto the adsorbent surface was determined at 25°C using equation (11), with an equilibration time (t) of 180 minutes. Equation (11) relates the initial concentration (Co) and equilibrium concentration (Ce) of Cr (VI) ions.

To investigate the adsorption process at different initial concentrations (Co) of Cr (VI) ions, the values of Ce and the rate constant (k) were calculated and compiled in Table 4. The rate constant was then plotted against the natural logarithm of the ratio (Co/Ce), as depicted in Figure 12.

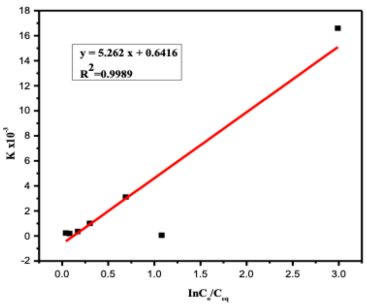


**Figure 12:** Adsorption kinetics of Cr (VI) ion on bionanomaterial

**Table 4:** Calculated rate constants (k) at different initial concentration Cr (vi) ions

| Initial conc. (mg/L) | $C_{eq}$ (mg/L) | Quantity of Cr (VI) Adsorbed (mg) | ln $C_o/C_{eq}$ | Rate constant ($kx10^{-3}min^{-1}$) |
|---|---|---|---|---|
| 5 | 0.25 | 4.75 | 2.99 | 16.6 |
| 10 | 5.18 | 4.82 | 0.65 | 3.6 |
| 20 | 15.13 | 4.87 | 0.27 | 1.5 |
| 40 | 35.04 | 4.96 | 0.13 | 0.7 |
| 60 | 56.08 | 3.92 | 0.06 | 0.3 |
| 80 | 76.84 | 3.16 | 1.08 | 0.06 |
| 100 | 97.18 | 2.82 | 0.04 | 0.22 |

Remarkably, the plot of the rate constant (k) against ln (Co/Ce) resulted in a straight line, indicating that the adsorption of Cr (VI) ions on the adsorbent surface follows first-order reaction kinetics. This implies that the rate of the adsorption process is directly proportional to the concentration gradient between Co and Ce.

## 4 CONCLUSION

This study investigated the adsorption mechanism of oxyanion chromium on ball-milled activated carbon derived from *Calotropis procera*. The BET surface area analysis revealed a remarkable increase in surface area from 302 $m^2/g$ to 578 $m^2/g$ after ball milling. FTIR analysis confirmed the presence of functional groups capable of attaching to Cr(VI) ions. SEM analysis demonstrated an irregular surface with larger holes and cave-like openings, which facilitated the adsorption of the metal ion.

Optimization of various parameters, including pH 2, contact time (180 min), adsorbent dosage (3 g), initial Cr(VI) concentration (40 ppm), and temperature (60°C), was conducted for the adsorption of Cr(VI) on the bionanomaterial. Thermodynamic analysis indicated that the adsorption process was endothermic and spontaneous, as evidenced by positive ΔH and negative ΔG values. The adsorption process followed first-order kinetics, and the experimental data best fit the Langmuir adsorption isotherm.

## 5 ACKNOWLEDGEMENT

The authors gratefully acknowledge the financial support provided by the Andhra Pradesh Pollution Control Board (APPCB), Andhra Pradesh, for this research work (Lr.No.APPCB/RFS/UH3/2019).

## REFERENCES

1) M. Singh, D. P. Tiwari, and M. Bhagat, Adsorption of Cr(VI) Ions using Activated Carbon Produced from Indian Water Chestnut (Trapa natans) Peel Powder, *Asian Journal of Chemistry*, 32, *4*, 876 (2020)URL https://doi.org/10.14233/ajchem.2020.22482.
2) X. Guo, A. Liu, A. Liu, X. Niu, M. Jiang, M. Jiang, and X. Liu, Adsorption Mechanism of Hexavalent Chromium on Biochar: Kinetic, Thermodynamic, and Characterization Studies, *ACS Omega*, 5, *42*, 27323 (2020)URL https://doi.org/10.1021/acsomega.0c03652.
3) T. Dula, K. Siraj, and S. A. Kitte, Adsorption of Hexavalent Chromium from Aqueous Solution Using Chemically Activated Carbon Prepared from Locally Available Waste of Bamboo (Oxytenanthera abyssinica), *ISRN Environmental Chemistry*, 2014, *438245*, 1 (2014)URL http://dx.doi.org/10.1155/2014/438245.
4) D. Yu, M. Wang, T. Tian, S. Lin, and P. Xu, The Effect of Hexavalent Chromium on the Incidence and Mortality of Human Cancers: A Meta-Analysis Based on Published Epidemiological Cohort Studies, *Frontiers in Oncology*, 9, *24*, 1 (2019)URL https://doi.org/10.3389/fonc.2019.00024.
5) E. Atangana and P. J. Oberholster, Mathematical modeling and stimulation of thermodynamic parameters for the removal for Cr6+ from wastewater using chitosan cross-linked glutaraldehyde adsorbent, *Alexandria Engineering Journal*, 59, *4*, 1931 (2020)URL https://doi.org/10.1016/j.aej.2019.12.012.
6) World Health Organization: Background document for development of WHO Guidelines for drinking-water quality, (2020).
7) A. Venkatesan, N. Ramalakshmi, and G. Vidhya, Adsorption of Fe3+ Ion from Aqueous Solution by Activated Carbon Prepared from Leucas aspera: Thermodynamic, Kinetic and Equilibrium Approach, *Asian Journal of Chemistry*, 29, *3*, 617 (2017)URL https://doi.org/10.14233/ajchem.2017.20276.
8) A. Muhammad, A. U. H. A. Shah, and S. H. Bilal, Effective Adsorption of Hexavalent Chromium and Divalent Nickel Ions from Water through Polyaniline, Iron Oxide, and Their Composites, *Applied Sciences*, 10, *8*, 2882 (2020)URL https://doi.org/10.3390/app10082882.
9) F. Kiliçel and H. S. Karapinar, Preparation and Characterization of Activated Carbon Produced from Eriobotrya japonica Seed by Chemical Activation with ZnCl2, *Asian Journal of Chemistry*, 30, *8*, 1823 (2018)URL https://doi.org/10.14233/ajchem.2018.21329.
10) J. Joseph, P. Olupot, W. E. Menya, and H. M. Kalibbala, Synthesis and Application of Granular Activated Carbon from Biomass Waste Materials for Water Treatment: A, *Review. Journal of Bioresources and Bioproducts*, 6, 292 (2021)URL https://doi.org/10.1016/j.jobab.2021.03.003.
11) H. Pirayesh, H. Khanjanzadeh, and A. Salari, Effect of using walnut/almond shells on the physical, mechanical properties and formaldehyde emission of particleboard, *Composites Part B: Engineering*, 45, *1*, 858 (2013)URL http://dx.doi.org/10.1016/j.compositesb.2012.05.008.
12) L. C. Clementin, C. Meng, P. S. Fennell, and J. P. Hallett, Efficient Fractionation of Lignin- and Ash-Rich Agricultural Residues Following Treatment With a Low-Cost Protic Ionic Liquid, *Frontiers in Chemistry*, 7, *246*, 1 (2019)URL https://doi.org/10.3389/fchem.2019.00246.
13) Y. X. Gan, Activated Carbon from Biomass Sustainable Sources, *C*, 7, *2*, 39 (2021)URL https://doi.org/10.3390/c7020039.
14) I. Moulefera, F. J. García-Mateos, A. Benyoucef, J. M. Rosas, J. Rodríguez-Mirasol, and T. Cordero, Effect of Co-solution of Carbon Precursor and Activating Agent on the Textural Properties of Highly Porous Activated Carbon Obtained by Chemical Activation of Lignin With H3PO4, *Frontiers in Materials*, 7, *153*, 1 (2020)URL https://doi.org/10.3389/fmats.2020.00153.
15) S. M. Yakout and G. S. El-Deen, Characterization of activated carbon prepared by phosphoric acid activation of olive stones, *Arabian Journal of Chemistry*, 9, *9*, S1155 (2016)URL http://dx.doi.org/10.1016/j.arabjc.2011.12.002.

16) M. N. Chai and M. I. N. Isa, The Oleic Acid Composition Effect on the Carboxymethyl Cellulose Based Biopolymer Electrolyte, *Journal of Crystallization Process and Technology*, 03, *01*, 1 (2013)URL https://doi.org/10.4236/jcpt.2013.31001.
17) F. J. Rodríguez-Vidal, B. Ortega-Azabache, Ángela González-Martínez, and A. Bellido-Fernández, Comprehensive characterization of industrial wastewaters using EEM fluorescence, FT-IR and 1H NMR techniques, *Science of The Total Environment*, 805, *805*, 150417 (2022)URL https://doi.org/10.1016/j.scitotenv.2021.150417.
18) B. Manoj, Role of Infrared Spectroscopy in Coal Analysis-An Investigation, *American Journal of Analytical Chemistry*, 5, 367 (2014)URL https://doi.org/10.4236/ajac.2014.56044.
19) Ş. Parlayici and E. Pehlivan, Comparative study of Cr(VI) removal by bio-waste adsorbents: equilibrium, kinetics, and thermodynamic, *Journal of Analytical Science and Technology*, 10, *1*, 1 (2019)URL https://doi.org/10.1186/s40543-019-0175-3.
20) G. B. Adebayo, H. I. Adegoke, and S. Fauzeeyat, Adsorption of Cr(VI) ions onto goethite, activated carbon and their composite: kinetic and thermodynamic studies, *Applied Water Science*, 10, *9*, 1 (2020)URL https://doi.org/10.1007/s13201-020-01295-z.
21) R. Labied, O. Benturki, A. Y. E. Hamitouche, and A. Donnot, Adsorption of hexavalent chromium by activated carbon obtained from a waste lignocellulosic material (Ziziphus jujuba cores): Kinetic, equilibrium, and thermodynamic study, *Adsorption Science & Technology*, 36, *3-4*, 1066 (2018)URL https://doi.org/10.1177/0263617417750739.
22) P. M. Thabede, N. D. Shooto, T. Xaba, and E. B. Naidoo, Sulfuric Activated Carbon of Black Cumin (Nigella sativa L.) Seeds for the Removal of Cadmium(II) and Methylene Blue Dye, *Asian Journal of Chemistry*, 32, *6*, 1361 (2020)URL https://doi.org/10.14233/ajchem.2020.22597.
23) V. K. Gupta, D. Pathania, and S. Sharma, Adsorptive remediation of Cu(II) and Ni(II) by microwave assisted H3PO4 activated carbon, *Arabian Journal of Chemistry*, 10, *2*, S2836 (2017)URL https://doi.org/10.1016/j.arabjc.2013.11.006.
24) M. A. Ahmad, N. A. A. Puad, and O. S. Bello, Kinetic, equilibrium and thermodynamic studies of synthetic dye removal using pomegranate peel activated carbon prepared by microwave-induced KOH activation, *Water Resources and Industry*, 6, 18 (2014)URL http://dx.doi.org/10.1016/j.wri.2014.06.002.